An Eigenfrequency-Constrained Topology Optimization Method with Design Variable Reduction

Wenchang Liu – Chaohua Wu* – Xingan Chen

Wuhan University of Technology, School of Mechanical and Electronic Engineering, China

The dynamic response of structures heavily relies on eigenfrequency, so the optimization of eigenfrequency is valuable in various working conditions. The bi-directional evolutionary structural optimization (BESO) method has been widely applied due to its ability to eliminate grayscale elements. Based upon BESO, this paper introduces a topology optimization method that incorporates eigenfrequency constraints and reduces the number of design variables. In this method, the optimization objective was to minimize compliance. The Lagrange multiplier was used to introduce eigenfrequency constraints, allowing for coordinated control of compliance and eigenfrequency. To prevent oscillation during the optimization process, the sensitivity was normalized. Additionally, to achieve faster convergence, the variables were reduced after meeting volume constraints. The numerical examples demonstrate the effectiveness of this method in increasing the eigenfrequency of the structure and avoiding resonance.

Keywords: Eigenfrequency constraint, topology optimization, bi-directional evolutionary structural optimization, design variable reduction; Lagrange multiplier method

Highlights
- *The eigenfrequency constraint was introduced through the Lagrange multiplier method.*
- *To obtain faster convergence, the variables were reduced after meeting volume constraints.*
- *The first-order natural frequency was increased by 42 % and 26.7 % in 2D numerical examples and 3D numerical examples respectively.*

0 INTRODUCTION

Topology optimization is an optimization algorithm for material distribution. Compared with the traditional optimization methods, sufficient freedom is the biggest advantage of topology optimization, which provides a reliable and convenient solution for developing high-performance structures and obtaining the best material layouts [1] to [3].

After more than decades of research and development, the practicality of topology optimization has been fully proven. At present, continuum topology optimization methods mainly include Solid Isotropic Material with Penalization Method (SIMP), Level Eet Method (LSM), Evolutionary Structural Optimization (ESO), Bi-directional Evolutionary Structural Optimization (BESO), etc. [4] and [5].

The SIMP method was proposed by Bendsøe and Kikuchi [6], which based on the ideal of discretizing the design domain and relating the density and materials. This means that there is no material, or it is a solid material when the density value is 0 or 1. The variation of element density values between 0 and 1 leads to the presenceof intermediate density elements, which is irrelevant in practical engineering. To address this issue, Rozvany et al. [7] proposed a density penalty scheme, which can update the element density towards 0 and 1 to obtain an approximate 0-1

structure. Sigmund [8] proposed a sensitivity filtering method to eliminate the checkerboard pattern and mesh dependency, which makes SIMP more stable. Osher and Sethian [9] proposed the concept of a level set function, Sethian and Wiegmann [10] first to apply this method to topology optimization; it updates the structure through the continuous evolution of the level set function and obtains clear and smooth boundaries. The method has a slow convergence speed, and it is not easy to obtain hole structures. The ESO method was proposed by Xie and Steven [11], which based on the ideal of gradually removing less efficient materials until the material requirements are met; its update concept is simple and clear, completely different from traditional mathematical programming algorithms. However, due to the possibility of mistakenly deleting elements during the optimization process to obtain local optima, Huang and Xie [12] improved this method to BESO. In this method, the sensitivity information of each element needs to be calculated and then sorted. The threshold is determined based on the volume fraction of each step. The elements with sensitivity numbers greater than the threshold are retained as solid elements, while elements with sensitivity numbers less than the threshold are deleted. Even if an element becomes a void element by deletion, its sensitivity information is still preserved and can be reinstated as a solid element in subsequent

iterations, ensuring that the optimization result is the optimal solution.

Topology optimization has also been widely applied to avoid structural resonance. Munk et al. [13] studied the problem of frequency topology optimization under dynamic loads, and proposed a topology optimization method that can enhance the selected frequency and the reduce gap between frequencies. Li et al. [14] proposed a modified frequency band-constrained Heaviside function, which is continuously differentiable and beneficial for sensitivity analysis. The numerical examples demonstrate that this method can maximize the eigenfrequency of the structure. Du et al. [15] carried out research on fault safety topology optimization based on independent continuous mapping (ICM) and expanded it to the realm of frequency optimization. Kang, et al. [16] proposed a topology optimization method for large-scale frequency constraints. Li, et al. [17] proposed a topology optimization method for frequency optimization with periodic structures and reduced the amount of calculation in the process of frequency optimization by utilizing dimension reduction technology. Leader, et al. [18] considered both stress and frequency constraints and utilized the Jacobi-Davidson eigenvalue solving method to solve the natural frequency problem. Wang et al. [19] established a dynamic topology optimization model for long-span continuum, effectively improving the first-order frequency. Xu et al. [20] proposed a frequency optimization problem with casting constraints, which can effectively obtain convergent solutions when dealing with frequency maximization problems. Su and Liu [21] studied the topology optimization of a coupled stress continuum to maximize the eigenfrequency, and also demonstrated the influence of eigen length on the results of eigenfrequency optimization. Ferrari et al. [22] proposed a frequency optimization method linked to a multi-mesh eigenvalue solver, greatly saving computational costs. Guan, et al. [23] proposed a multi-constraint topology optimization method with stress, displacement, and frequency constraints. Kim et al. [24] applied the topology optimization method to increase the frequency and reduce the noise of the steel wheel. Duan et al. [25] proposed a topology optimization method that can increase the frequency in a limited way while meeting the manufacturing constraints. Oh et al. [26] proposed a topology optimization method to maximize the operating frequency range of hyperbolic elastic meta-material and explained the mechanical knowledge of the model in detail. Vicente et al. [27] proposed a parallel topology optimization method for

frequency optimization to find the optimal layout of materials from both macro- and micro-perspectives.

In addition, how to reduce the number of iteration steps and accelerate the convergence process are also a problem that need to be solved in topology optimization. Zheng et al. [28] introduced a freedom reduction mechanism in topology optimization, effectively accelerating the convergence process and saving the calculation cost. Jia et al. [29] combined ESO with LSM, which can reduce the number of iteration steps by automatically generating holes in the low-strain energy region near the node. Lian et al. [30] added a hierarchical mesh refinement algorithm into the moving morphable component (MMC) algorithm to improve convergence speed. Joo and Jang [31] proposed a deep neural network topology optimization algorithm, which can improve the convergence speed by obtaining the history of intermediate designs. Li and Zhang [32] used high noise and unbiased random gradients to update design variables and expedite the convergence process. Du et al. [33] shared a set of efficient topology optimization Matlab codes, which resulted in faster convergence speeds by removing the freedom not belonging to the transmission path in the finite element analysis. Yang et al. [34] proposed an adaptive step size strategy that multiplies the speeds of different nodes by different step sizes, which can accelerate convergence and also reduce mesh dependency. According to the characteristics of the BESO algorithm, Lin et al. [35] proposed a dynamic evolution strategy to accelerate convergence in topology optimization. Ren, et al. [36] used faster model reduction methods to enhance convergence speed.

In this paper, an eigenfrequency-constrained topology optimization method with design variable reduction is proposed, which can rapidly converge while increasing the eigenfrequency. Numerical examples demonstrate the effectiveness of this method.

1 TOPOLOGY OPTIMIZATION WITH EIGENFREQUENCY CONSTRAINTS

1.1 Problem Statement

When topology optimization is applied to structural design, volume is usually taken as the constraint, and the minimum compliance is taken as the optimization objective. This reflects the fact that stiffness is an extremely important objective in traditional structural design concepts. However, the topology optimization model will be multi-objective, multi-constraint and

include other related conditions to meet engineering requirements and address complex working conditions.

In recent years, constraints other than volume introduced in topology optimization can be broadly divided into two categories. One type is related to manufacturing, including maximum and minimum size constraints, connectivity constraints, hole size constraints, hole number constraints, inclination angle constraints, and self-supporting constraints; The other type of constraint is functionality, such as displacement constraints, stress-strain constraints, fatigue constraints, and damage constraints.

As is well known, avoiding resonance is one of the important design objectives in structural design; it can be avoided by increasing the eigenfrequency of the structure. BESO is widely applied due to its simple concept and clear boundaries. The BESO topology optimization model with eigenfrequency constraints can be described mathematically as follows,

$$
\begin{cases}
\text{find} \quad \mathbf{X} = \left(x_{11}, x_{12}, x_{13}, \cdots x_{ij}\right) \\
\qquad i = 1, 2, ..., m; \quad j = 1, 2, ..., n; \\
\text{min} \quad C(\mathbf{X}) = \dfrac{1}{2}\mathbf{U}^T\mathbf{K}\mathbf{U} \\
\text{s.t.} \quad \mathbf{K}\mathbf{U} = \mathbf{F} \\
\qquad \left(\mathbf{K} - \omega_n^2\mathbf{M}\right)\mathbf{u}_n = 0 \\
\qquad V = qV_0 \\
\qquad x_{ij} = x_{\min} \text{ or } 1 \\
\qquad WY < \omega_n
\end{cases}, \quad (1)
$$

where the $\mathbf{X}$ is the design variable, x_{ij} is the ijth elemental density with a value of either 1 for solid or $x_{\min}$ (0.001 in this paper) for void, compliance $C(\mathbf{X})$ is an objective function, $\mathbf{K}$ is the global stiffness matrix, $\mathbf{U}$ is the global displacement vector, $\mathbf{F}$ is the force vector, $\mathbf{M}$ is the global mass matrix, $\mathbf{u}_n$ is the eigenvector corresponding to ω_n, V_0 is the initial volume of structure, q is reserved volume ratio, V is the final structural volume, ω_n is nth natural frequency, WY is frequency constraint value.

The following Rayleigh quotient indicate the relationship between ω_n and $\mathbf{u}_n$, as follows (Eq. (2)),

$$
\omega_n^2 = \frac{\mathbf{u}_n^T\mathbf{K}\mathbf{u}_n}{\mathbf{u}_n^T\mathbf{M}\mathbf{u}_n}. \quad (2)
$$

1.2 Material Interpolation Scheme

The material interpolation scheme applied in calculating compliance is expressed as follows, Eqs. (3) and (4):

$$
E_{ij} = E_0 x_{ij}^{penal}, \quad (3)
$$

$$
\mathbf{K}_{ij} = \mathbf{K}_0 x_{ij}^{penal}, \quad (4)
$$

where the E_{ij} is the ijth elemental Young's modulus, E_0 is the Young's modulus of the solid element, *penal* (*penal*=3 in this paper) is a value used for the density penalty. When *penal*≤2, there is a large amount of porous material, and the optimized structure cannot be manufactured. When *penal*≥3.5, there is no significant change in the final topology result. When *penal*≥4, it will make the calculation very slowly. Therefore, *penal*=3 in this paper. $\mathbf{K}_{ij}$ is the stiffness matrix of the ijth element, $\mathbf{K}_0$ is the stiffness matrix of the solid element.

To avoid local vibration modes during finite element analysis and the solution of frequencies, the material interpolation scheme is defined as follows, in Eqs. (5) and (6):

$$
\rho\left(x_{ij}\right) = x_{ij}\rho_0, \quad (5)
$$

$$
E\left(x_{ij}\right) = \left[\frac{x_{\min} - x_{\min}^{penal}}{1 - x_{\min}^{penal}}\left(1 - x_{ij}^{penal}\right) + x_{ij}^{penal}\right]E_0, \quad (6)
$$

where ρ_0 and $\rho(x_{ij})$ denote respectively the material density of the solid and ijth.

1.3 Sensitivity Analysis

1.3.1 Lagrange Multiplier Method

In BESO topology optimization, constraints other than volume can be added with Lagrange multiplier method; the objective function is expressed as follows, Eq. (7):

$$
f = C + \lambda\left(WY - \omega_n\right), \quad \lambda \geq 0, \quad (7)
$$

where λ is the Lagrangian multiplier.

In the BESO method, the Lagrange multiplier method has been widely applied to solve multi-constraint problems. For instance, Huang and Xie [37] utilized this method to address displacement constraints, while Fan et al. [38] employed it to tackle stress constraints. The Lagrange multiplier method is suitable for obtaining optimal solutions under multiple constraints. It is easy to perform the sensitivity analysis by introducing a Lagrange multiplier to incorporate inequality constraints.

1.3.2 Sensitivity Number

In the BESO method, it is necessary to sort the sensitivity of each element and then update the

variables by determining a threshold based on volume constraints. According to Eq. (7), objective function sensitivity can be obtained as follows, Eq. (8):

$$\frac{\partial f}{\partial x_e} = \frac{\partial C}{\partial x_e} + \lambda \frac{\partial \omega_n}{\partial x_e}. \tag{8}$$

According to Eqs. (1), (3) and (4), compliance sensitivity can be obtained, as follows, Eq. (9):

$$\frac{\partial C}{\partial x_e} = -\frac{1}{2} penal \, x_e^{penal-1} \mathbf{U}_e^T \mathbf{K}_0 \mathbf{U}_e, \tag{9}$$

where $\mathbf{U}_e$ is the displacement vector of eth. According to Eqs. (5) and (6), Eqs. (10) and (11) can be obtained by the derivation calculus, as follows:

$$\frac{\partial \mathbf{M}}{\partial x_{ij}} = \mathbf{M}_0, \tag{10}$$

$$\frac{\partial \mathbf{K}}{\partial x_{ij}} = \frac{1-x_{\min}}{1-x_{\min}^{penal}} penal \, x_{ij}^{penal-1} \mathbf{K}_0, \tag{11}$$

where $\mathbf{M}_0$ is the mass matrix of the solid element. Frequency sensitivity can obtained based on Eqs. (10) and (11), as follows, Eq. (12):

$$\frac{\partial \omega_n}{\partial x_e} = \frac{1}{2\omega_n} \mathbf{u}_n^T \left(\frac{1-x_{\min}}{1-x_{\min}^{penal}} penal \, x_e^{penal-1} \mathbf{K}_0 - \omega_n^2 \mathbf{M}_0 \right) \mathbf{u}_n. \tag{12}$$

According to Eqs. (8), (9) and (12), complete objective function sensitivity can obtained, as follows, Eq. (13):

$$\frac{\partial f}{\partial x_e} = -\frac{1}{2} penal \, x_e^{penal-1} \mathbf{U}_e^T \mathbf{K}_0 \mathbf{U}_e$$
$$-\lambda \frac{1}{2\omega_n} \mathbf{u}_n^T \left(\frac{1-x_{\min}}{1-x_{\min}^{penal}} penal x_e^{penal-1} \mathbf{K}_0 - \omega_n^2 \mathbf{M}_0 \right) \mathbf{u}_n. \tag{13}$$

Finally, the sensitivity number can be obtained based on the sensitivity analysis, as follows, Eq. (14):

$$\alpha_e = -\frac{1}{penal} \frac{\partial f}{\partial x_e}, \tag{14}$$

where α_e is the sensitivity number of eth.

1.3.3 Variable Update Principle

The filtering scheme can be used to avoid checkerboard patterns and mesh-dependency, as follows, Eq. (15):

$$\begin{cases} \Delta_{ij,lk} = \sqrt{(l-i)^2 + (k-j)^2} \\ \mu_{e,lk} = max\{0, r_{min} - \Delta_{e,lk}\}, \\ \alpha_e^{\,t} = \dfrac{\sum_{l=1}^{m}\sum_{k=1}^{n} \mu_{e,lk}\alpha_{lk}}{\sum_{l=1}^{m}\sum_{k=1}^{n} \mu_{e,lk}} \end{cases} \tag{15}$$

where $\Delta_{ij,lk}$ is the distance between the centers of elements lk and ij; $\mu_{e,lk}$ is a weight factor, r_{min} is a filter radius, t is current iteration steps. It is effective to ensure a smoother optimization process and improve the stability of the optimization model by averaging three historical sensitivity number for averaging, as follows, Eq. (16):

$$\alpha_e^{\,t} = \alpha_e^{\,t} + \alpha_e^{\,t-1} + \alpha_e^{\,t-2}, \tag{16}$$

where λ is 0 when frequency constraints are met. The objective function aims to minimize compliances, which is equivalent to the original model. λ can be updated a value that satisfies the constraints can be updated until the constraint is satisfied.

The update method for the Lagrange multiplier is expressed as follows, Eqs. (17) and (18):

$$s_{t+1} = 0.5(s_{\min} + s_t), \tag{17}$$

$$\lambda_{t+1} = \frac{1-s_{t+1}}{s_{t+1}}, \tag{18}$$

where s_t is a constant with a value range of $s_{\min}$ to 1, $s_{\min}$ is a very small positive number; s_{t+1} and λ_{t+1} can be updated to 1 and 0, respectively, when the constraint is met.

An appropriate Lagrange multiplier updating strategy is of great importance for achieving speed and accuracy. Lagrange multiplier updating strategies may vary in different constraint problems, which requires specific analysis according to the individual problems. It is particularly associated with the sensitivity to Lagrange multipliers and the nonlinearity of the optimization model. The oscillation is normal when using the Lagrange multiplier updating strategy optimization process. However, convergence becomes difficult when faced with numerous and large oscillations.

Therefore, the normalization strategy needs to be adopted to avoid oscillation, as follows, Eq. (19):

$$\alpha_e^{\,t} = \frac{\alpha_e^{\,t} - \alpha_{\min}^{\,t}}{\alpha_{\max}^{\,t} - \alpha_{\min}^{\,t}}, \tag{19}$$

where $\alpha_{\min}^t$ and $\alpha_{\max}^t$ is the minimum and maximum sensitivity value in the tth iteration step, respectively.

During the optimization process, the variation pattern of volume is expressed, as follows, Eq. (20):

$$V^t = \max\left\{V, V^{t-1}(1 - ER)\right\}, \qquad (20)$$

where V^t is volume value in the tth iteration step, ER is the volume evolution rate.

The convergence condition is the value of five relative changes in compliance less than 0.01, as follows, Eq. (21):

$$\nabla f = \frac{\left|\sum_{t-4}^{t} c_t - \sum_{t-9}^{t-5} c_t\right|}{\sum_{t-4}^{t} c_t} < 0.01, \qquad (21)$$

where ∇f is the value of 5 relative changes in compliance, c_t is the compliance in the tth iteration step.

2 2D NUMERICAL EXAMPLES

As shown in Fig. 1, the design domain is a 180:90 rectangular region for a prescribed volume fraction of $V = 50$ %. The beam is simply supported at both ends and vertically loaded ($P = 10$ N) in the middle of its lower edge. The rectangular design domain is divided into 180×90 four-node plane stress elements. Young's modulus $E = 1$ MPa, the volume evolution rate $ER = 0.01$, filter radius $r_{\min}$ is twice the length of the element side, Poisson's ratio $v = 0.3$ and mass density $\rho = 0.001$ kg/m³. The optimization objective is to minimize the compliance while satisfying the constraint on the first-order eigenfrequency.
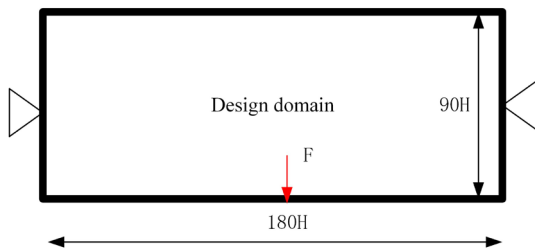
Fig. 1. *The design domain of 2D numerical example*

The optimization results can be obtained by setting different optimization parameters, as shown in Fig. 2.

The optimal topology without any eigenfrequency constraint is shown in Fig. 2a for comparison. When ω_1 is constrained to be 150 rad/s, 155 rad/s, 170 rad/s, 178 rad/s, 188 rad/s, the resulting topologies are shown in Fig. 2b to f. Their compliances are 547.9578,

681.4366, 812.0577, 710.2652, 1096.7411. Their first-order eigenfrequency are 150.8144 rad/s, 155.5822 rad/s, 175.5030 rad/s, 184.1129 rad/s, 188.7140 rad/s.

From Fig. 2b to f, it can be seen that the first-order eigenfrequency increases gradually after the eigenfrequency constraint is introduced, which can meet the constraint conditions. When the first-order eigenfrequency increases gradually, the compliance also increases gradually. It can be seen that the stiffness is sacrificed while satisfying the eigenfrequency constraint.

Without introducing eigenfrequency constraints, the optimization process is shown in Fig. 3a, When the eigenfrequency constraint is $WY = 178$ rad/s, the optimization process is shown in Fig. 3b.

From Fig. 3a, it can be seen that the compliance C continuously increased without eigenfrequency constraints as the material is continuously removed. When the volume constraint is satisfied, the compliance C reaches its maximum value, and finally tend to be stable. The first-order eigenfrequency will initially increase and then decrease. During the entire optimization process, ω_1 will fluctuate obviously, but it will eventually stabilize. C is stable growth, and there are no noticeable oscillations throughout the entire optimization process.

It can be seen from Fig. 3b that the topology optimization in the direction of satisfying the eigenfrequency constraint is carried out firstly when the eigenfrequency constraint is $WY = 178$ rad/s. Then the topology optimization is then performed in the direction of minimum compliance once the structure satisfies the eigenfrequency constraint. The entire optimization process involves a coordinated optimization of eigenfrequency constraints and minimum compliance. The Lagrange multiplier plays a coordinating role. In the continuous coordination, the local optimal solution satisfying the eigenfrequency constraint and the minimum compliance is finally obtained. During the mid-term stage of the optimization process, there will be a large oscillation. With the removal of the material, fluctuates near $WY = 178$ rad/s and eventually satisfies the constraints. At this time, the compliance is also converging.

In this example, $\omega_1 = 132.1478$ rad/s can be increased to $\omega_1 = 188.7140$ rad/s. The ω_1 is increased by 42 %. In practical engineering applications, the value of 42 % eigenfrequency increase is undoubtedly huge, which can effectively avoid structural resonance. When the design domain, material parameters and constraint conditions vary, the effect of frequency enhancement will be significantly different. However,

a) $WY = 0$ rad/s; $\omega_1 = 132.1478$ rad/s; $C = 521.2869$

b) $WY = 150$ rad/s; $\omega_1 = 150.8144$ rad/s; $C = 547.9578$

c) $WY = 155$ rad/s; $\omega_1 = 155.5822$ rad/s; $= 681.4366$

d) $WY = 170$ rad/s; $\omega_1 = 175.5030$ rad/s; $C = 812.0577$

e) $WY = 178$ rad/s; $\omega_1 = 184.1129$ rad/s; $C = 710.2652$

f) $WY = 188$ rad/s; $\omega_1 = 188.7140$ rad/s; $C = 1096.7411$
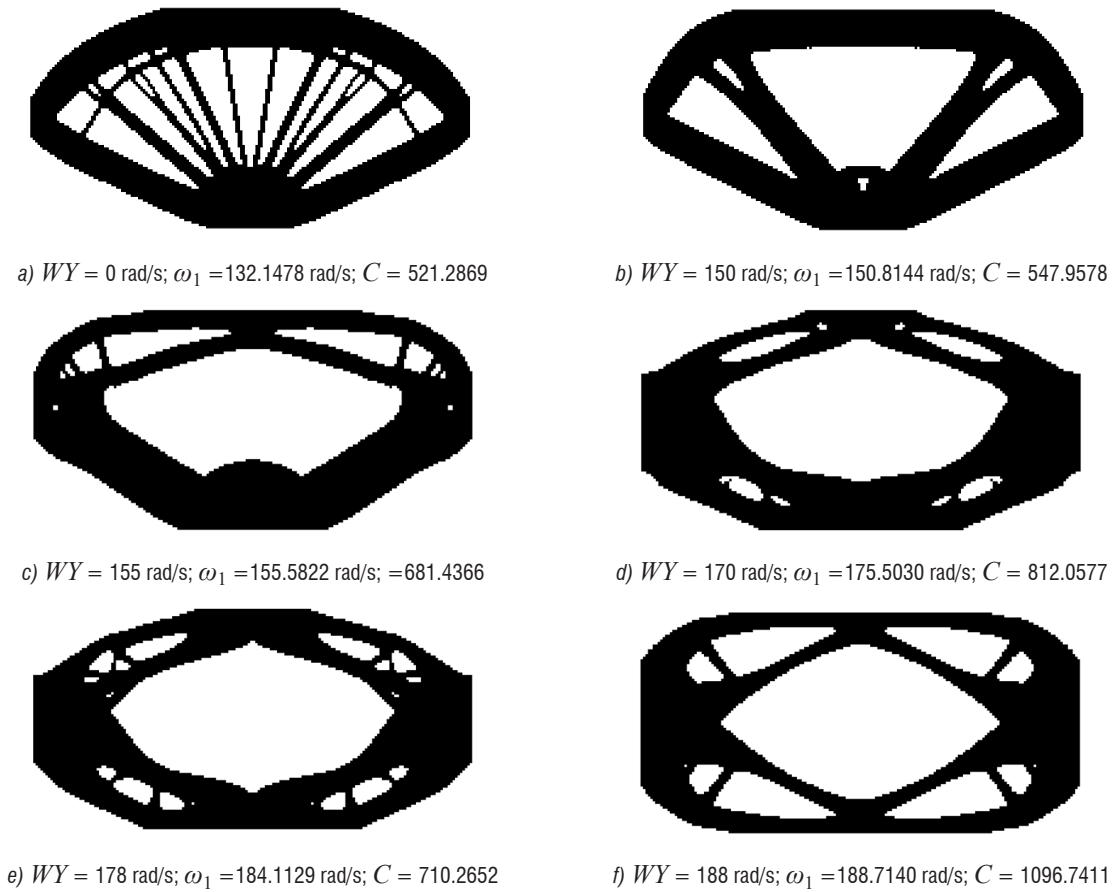
Fig. 2. *The optimization results of 2D numerical examples*
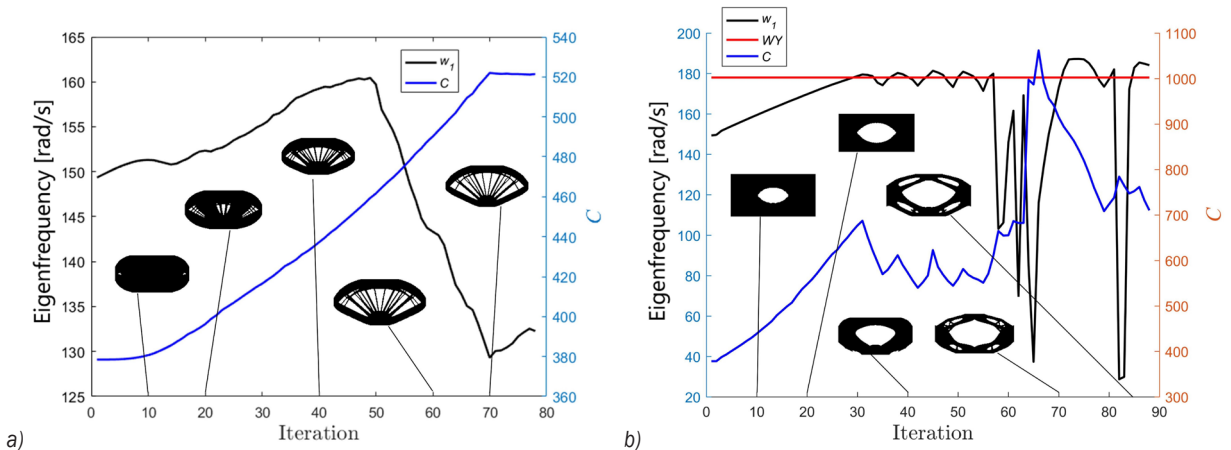
Fig. 3. *The optimization process of 2D numerical examples*

this method is undoubtedly a solution and can provide a reference for related designs.

3 DESIGN VARIABLE REDUCTION

In topology optimization, the large number of variables necessitates extensive calculations and results in a high degree of freedom. In topology optimization,
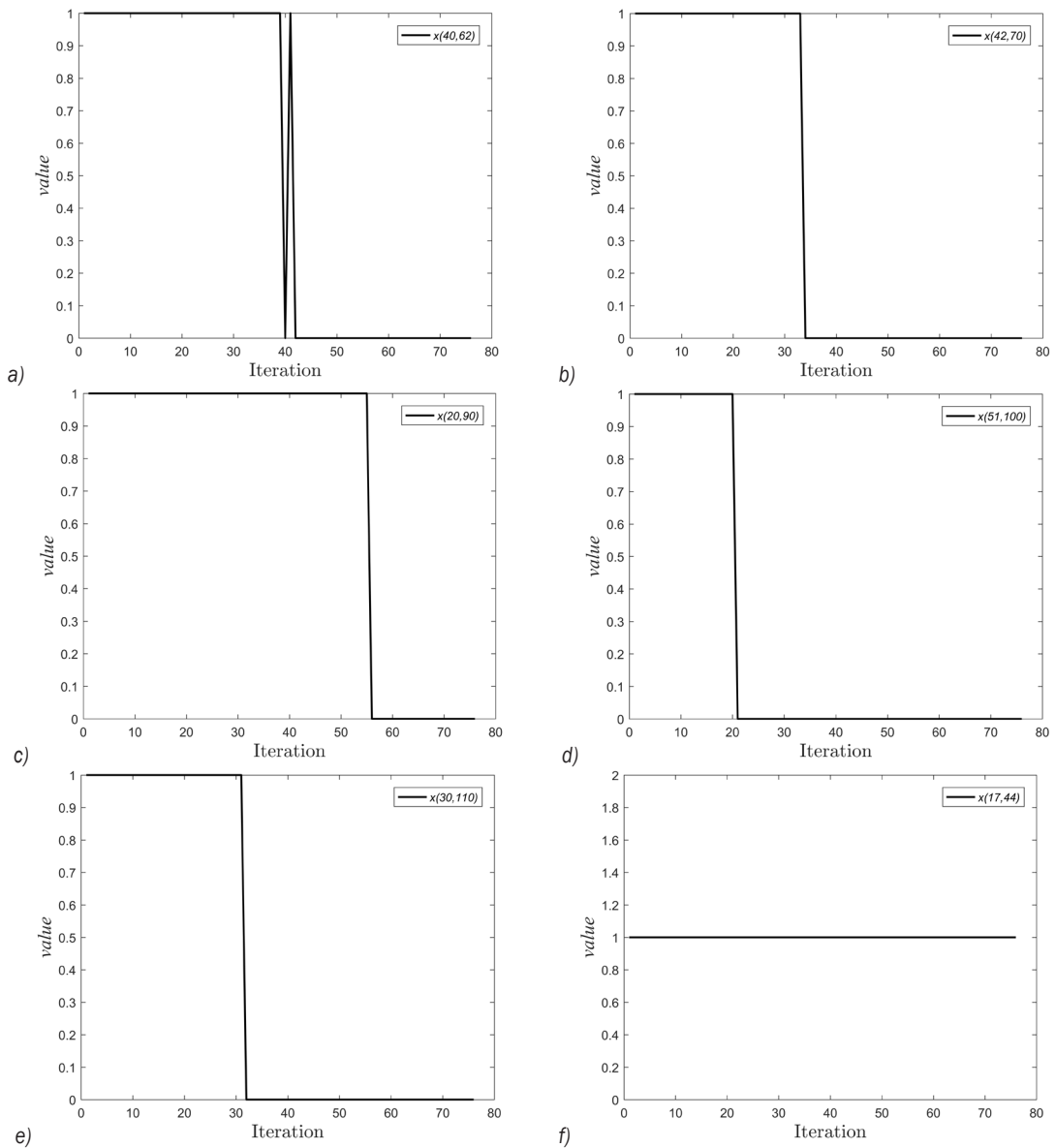
Fig. 4. *The change of different variables*

certain variables converge early and reach a stable state. Similarly, taking the simply supported beam in Section 2 as an example, when the eigenfrequency constraint is not introduced, the changes in some variables are shown in Fig. 4. Where the $X(i,j)$ is the ij^{th} elemental density.

It can be seen from Fig. 4 that different variables converge at different times: some converge early, and some converge later. This paper defines that when the value of the continuous 5-step variable does not change (that is, when Eq. (22) is satisfied), the

variable is a stable variable, and the variable that does not satisfy Eq. (22) is a free variable.

$$x_{ij}^{t} + x_{ij}^{t-1} + x_{ij}^{t-2} + x_{ij}^{t-3} + x_{ij}^{t-4} = 5 \text{ or } 5x_{min}. \quad (22)$$

When the topology optimization satisfies the volume constraint, the number of design variables can be reduced. This means that the stable variables remain unchanged and no longer participate in the variable update. The algorithm flowchart is shown in Fig. 5. For comparison, the simply supported beam in Section 3 is also utilized as an example. When

the eigenfrequency constraint is $WY = 178$ rad/s, the optimization process is shown in Fig. 6 using the algorithm depicted in Fig. 5.
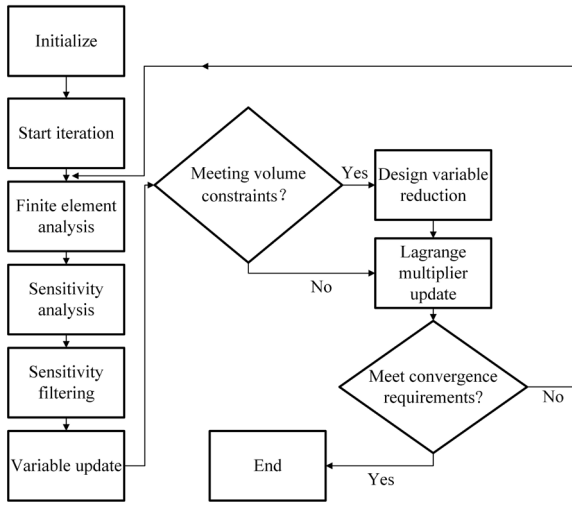
Fig. 5. *The algorithm flow chart*
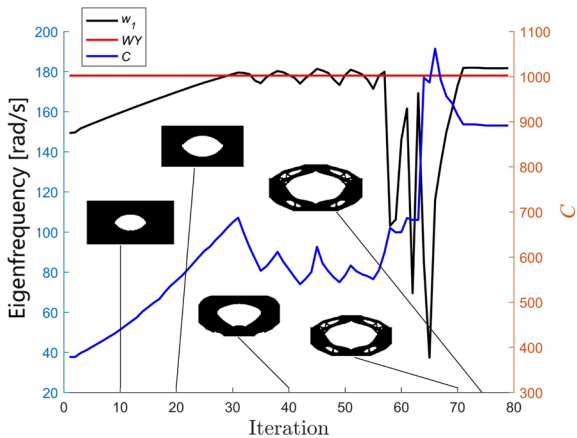
Fig. 6. *The optimization process by using the algorithm shown in Fig. 5*

It can be seen from Fig. 6 that when the design variable reduction mechanism is introduced, the entire optimization process can still obtain the results that meet the constraints, and the number of oscillations is significantly reduced.

This paper conducts a large number of numerical examples to compare the iterations required for convergence without the introduction of design variable reduction mechanism and with the introduction of design variable reduction mechanism. The comparison results are shown in Table 1 and Fig. 7.

It can be observed from Table 1 and Fig. 7 that the change trend of the number of iterations required

for convergence in both methods is essentially the same. However, there is a significant reduction in the number of iterations after the design variable is decreased. It has been proven that reducing the design variables can effectively decrease the number of iterations and speed up convergence.

Table 1. *Iterations required for convergence*

Eigenfrequen constraint [rad/s]	Iterations without variable reduction	Iterations with variable reduction
$WY = 150$	82	75
$WY = 155$	83	79
$WY = 170$	78	75
$WY = 178$	88	79
$WY = 188$	81	77
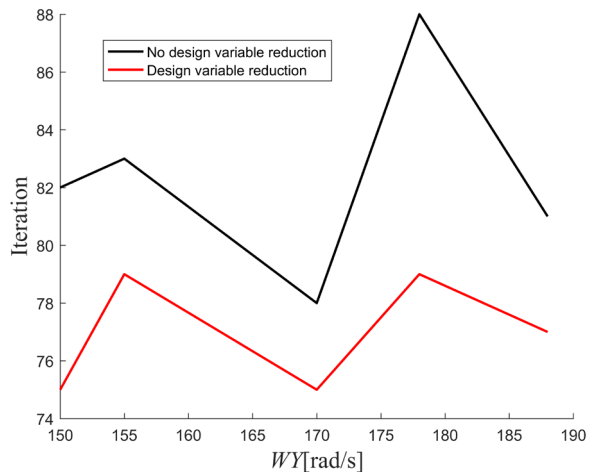
Fig. 7. *The comparison diagram of iterations*

4 3D NUMERICAL EXAMPLES

In the 2D example, the effectiveness of the eigenfrequency constrained topology optimization method with design variable reduction has been fully proved. Next, a 3D example is used for simple verification.

As shown in Fig. 8, the design domain is a $30:20:10$ cube region in which the degree of freedom of the intermediate nodes on both sides is restricted, and a concentrated load of 1 N is applied to the midpoint of the bottom surface.
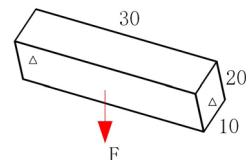
Fig. 8. *The design domain of 3D numerical examples*

The prescribed volume fraction is $V = 15$ %. The cube design domain is divided into $30 \times 20 \times 10$ four node plane stress elements. Young's modulus $E = 1$ MPa, volume evolution rate $ER = 0.01$, filter radius r_{min} is 1.5 times the element side length, Poisson's ratio $v = 0.3$ and mass density $\rho = 1$ kg/m³. The optimization objective is to minimize the compliance with the first-order eigenfrequency constrained. The number of iterations is abbreviated as it. The optimization results of the 3D numerical examples are shown in Fig. 9.

The optimal topology without any eigenfrequency constraint is shown in Fig. 9a for comparison. When ω_1 is constrained to be 285 rad/s, 290 rad/s, 295 rad/s, 300 rad/s, 330 rad/s, the resulting topologies are shown in Figs. 9b to f. Their compliances are 4.0722, 4.0208, 4.0060, 4.1454, 5.1104. Their first-order eigenfrequency are 299.4611 rad/s, 303.2690 rad/s, 306.1478 rad/s, 311.2603 rad/s, 339.2250 rad/s. Their iterations are 132, 129, 129, 138, 139.

It can be seen from Fig. 9 that the first-order eigenfrequency can be improved by introducing eigenfrequency constraints. In this example, $\omega_1 = 267.6767$ rad/s can be increased to $\omega_1 = 339.2250$ rad/s. The ω_1 is increased by 26.7 %. The number of iterations is within 140 steps, and the convergence speed is faster.

5 CONCLUSIONS

In this paper, an eigenfrequency constrained topology optimization method with design variable reduction is proposed. Based on BESO, the eigenfrequency constraint is introduced using the Lagrange multiplier, and the topology optimization is performed with the objective of minimizing compliance. After satisfying the volume constraint, the design variable is reduced, which can significantly decrease the number of iterations and expedite convergence. The first-order eigenfrequency can be increased by 42 % and 26.7

a) $WY = 0$ rad/s; $\omega_1 = 267.6767$ rad/s; $C = 3.6387$; $it = 200$ b) $WY = 285$ rad/s; $\omega_1 = 299.4611$ rad/s; $C = 4.0722$; $it = 197$

c) $WY = 290$ rad/s; $\omega_1 = 303.2690$ rad/s; $C = 4.0208$; $it = 198$ d) $WY = 295$ rad/s; $\omega_1 = 306.1478$ rad/s; $C = 4.0060$; $it = 200$

e) $WY = 300$ rad/s; $\omega_1 = 311.2603$ rad/s; $C = 4.1454$; $it = 201$ f) $WY = 330$ rad/s; $\omega_1 = 339.2250$ rad/s; $C = 5.1104$; $it = 203$
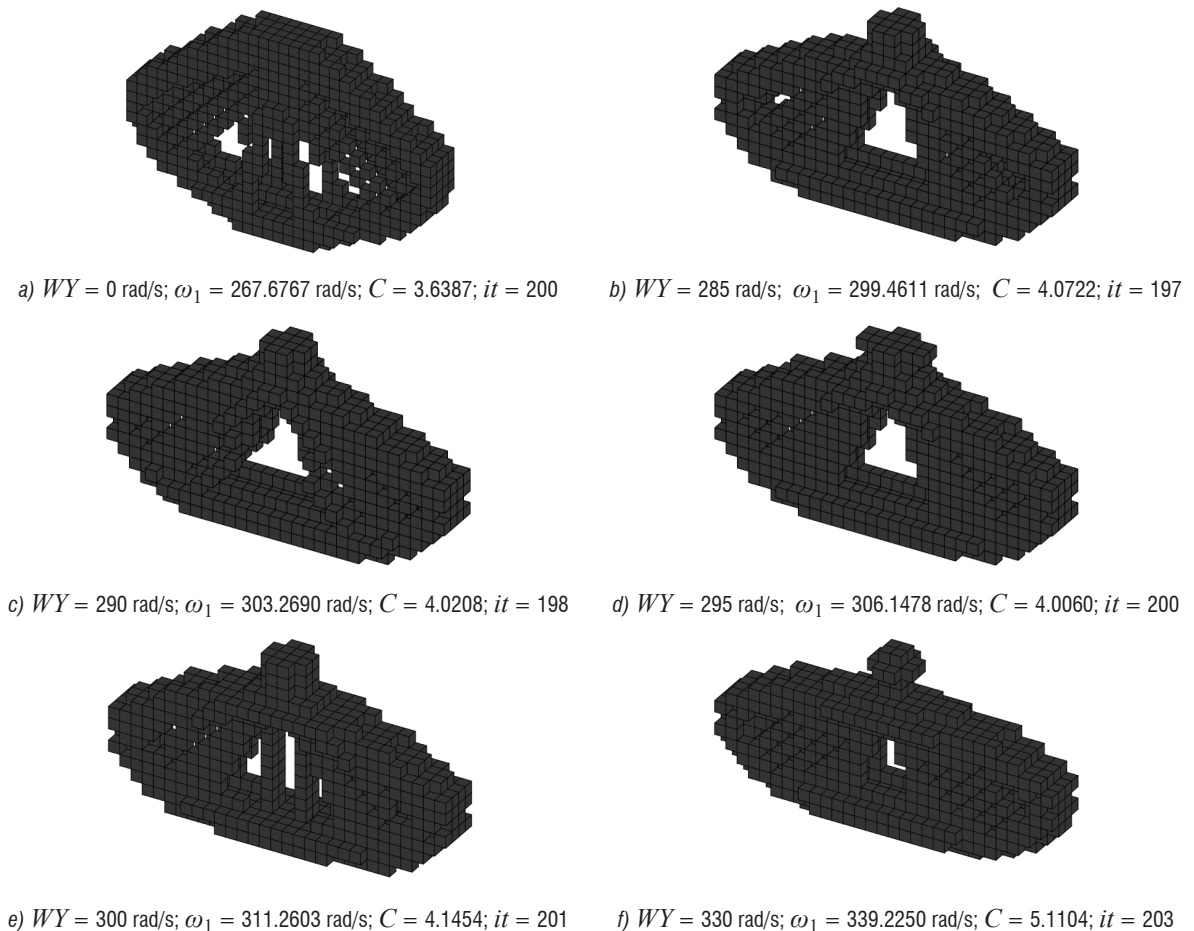
Fig. 9. *The optimization results of 3D numerical examples*

% in 2D numerical examples and in 3D numerical examples,respectively.

6 ACKNOWLEDGMENTS

7 REFERENCES

[1] Rosen, D.W. (2016). A review of synthesis methods for additive manufacturing. *Virtual and Physical Prototyping*, vol. 11, no. 4, p. 305-317, **DOI:10.1080/17452759.2016.1240208**.

[2] Liu, J., Gaynor, A.T., Chen, S., Kang, Z., Suresh, K., Takezawa, A., Li, L., Kato, J., Tang, J., Wang, C.C.L., Cheng, L., Liang, X., To, A.C. (2018). Current and future trends in topology optimization for additive manufacturing. *Structural and Multidisciplinary Optimization*, vol. 57, no. 6, p. 2457-2483, **DOI:10.1007/s00158-018-1994-3**.

[3] Meng, L., Zhang, W., Quan, D., Shi, G., Tang, L., Hou, Y., Piotr, B., Zhu, J., Gao, T. (2019). From topology optimization design to additive manufacturing: Today's success and tomorrow's roadmap. *Archives of ComputationalMethods in Engineering*, vol. 27, p. 805-830, **DOI:10.1007/s11831-019-09331-1**.

[4] Dilgen, C.B., Dilgen, S.B., Aage, N., Jensen, J.S.. (2019). Topology optimization of acoustic mechanical interaction problems: a comparative review. *Structural and Multidisciplinary Optimization*, vol. 60, no. 2, p. 779-801, **DOI:10.1007/s00158-019-02236-4**.

[5] Deaton, J.D., Grandhi, R.V. (2014). A survey of structural and multidisciplinary continuum topology optimization: post 2000. *Structural and Multidisciplinary Optimization*, vol. 49, no. 1, p. 1-38, **DOI:10.1007/s00158-013-0956-z**.

[6] Bendsøe, M.P., Kikuchi, N. (1988). Generating optimal topologies in structural design using a homogenization method. *Computer Methods in Applied Mechanics and Engineering*, vol. 71, no. 2, p. 197-224, **DOI:10.1016/0045-7825(88)90086-2**.

[7] Rozvany, G.I., Zhou, M., Birker, T. (1992). Generalized shape optimization without homogenization. *Structural Optimization*, vol. 4, p. 250-252, **DOI:10.1007/BF01742754**.

[8] Sigmund, O. (2001). A 99 line topology optimization code written in Matlab. Structural and Multidisciplinary Optimization, vol. 21, p. 120-127, **DOI:10.1007/s001580050176**.

[9] Osher, S., Sethian, J.A. (1988). Fronts propagating with curvature-dependent speed: Algorithms based on Hamilton-Jacobi formulations. *Journal of Computational Physics*, vol. 79, no. 1, p. 12-49, **DOI:10.1016/0021-9991(88)90002-2**.

[10] Sethian, J.A., Wiegmann, A. (2000). Structural boundary design via level set and immersed interface methods. *Journal of Computational Physics*, vol. 163, no. 2, p. 489-528, **DOI:10.1006/jcph.2000.6581**.

[11] Xie, Y.M., Steven, G.P. (1993). A simple evolutionary procedure for structural optimization. *Computers & Structures*, vol. 49, no. 5, p. 885-896, **DOI:10.1016/0045-7949(93)90035-C**.

[12] Huang, X., Xie, Y.M. (2007). Convergent and mesh-independent solutions for the bi-directional evolutionary structural optimization method. *Finite Elements in Analysis and Design*, vol. 43, no. 14, p. 1039-1049, **DOI:10.1016/j.finel.2007.06.006**.

[13] Munk, D.J., Vio, G.A., Steven, G.P. (2017). Novel moving isosurface threshold technique for optimization of structures under dynamic loading. *AIAA Journal*, vol. 55, no. 2, p. 638-651, **DOI:10.2514/1.J054692**.

[14] Li, Q., Wu, Q., Liu, J., He, J., Liu, S. (2021), Topology optimization of vibrating structures with frequency band constraints. *Structural and Multidisciplinary Optimization*, vol. 63, p. 1203-1218, **DOI:10.1007/s00158-020-02753-7**.

[15] Du, J.Z., Meng, F.W., Guo, Y.H., Sui, Y.K. (2020). Fail-safe topology optimization of continuum structures with fundamental frequency constraints based on the ICM method, *Acta Mechanica Sinica*, vol. 36, p. 1065-1077, **DOI:10.1007/s10409-020-00988-7**.

[16] Kang, Z., He, J., Shi, L., Miao, Z. (2020), A method using successive iteration of analysis and design for large-scale topology optimization considering eigenfrequencies. *Computer Methods in Applied Mechanics and Engineering*, no. 362, p. 112847, **DOI:10.1016/j.cma.2020.112847**.

[17] Li, M., Cheng, Z., Jia, G., Shi, Z. (2019), Dimension reduction and surrogate based topology optimization of periodic structures. *Composite Structures*, no. 229, p. 111385, **DOI:10.1016/j.compstruct.2019.111385**.

[18] Leader, M.K., Chin, T.W., Kennedy, G.J. (2019). High-resolution topology optimization with stress and natural frequency constraints. *AIAA Journal*, vol. 57, no. 8, p. 3562-3578, **DOI:10.2514/1.J057777**.

[19] Wang, Y., Qin, D., Wang, R., Zhao, H. (2021). Dynamic topology optimization of long-span continuum structures. *Shock and Vibration*, no. 2021, p. 1-9, **DOI:10.1155/2021/4421298**.

[20] Xu, B., Han, Y.S., Zhao, L., Xie. Y.M. (2019). Topology optimization of continuum structures for natural frequencies considering casting constraints. *Engineering Optimization*, vol. 51, no. 6, p. 941-960, **DOI:10.1080/0305215X.2018.1506771**.

[21] Su, W., Liu, S. (2016). Topology design for maximization of fundamental frequency of couple-stress continuum, *Structural and Multidisciplinary Optimization*, no. 53, p. 395-408, **DOI:10.1007/s00158-015-1316-y**.

[22] Ferrari, F., Lazarov, B.S., Sigmund. O. (2018). Eigenvalue topology optimization via efficient multilevel solution of the frequency response. *International Journal for Numerical Methods in Engineering*, vol, 115, no. 7, p. 872-892, **DOI:10.1002/nme.5829**.

[23] Guan, H., Chen, Y.J., Loo, Y.C., Xie, Y.M. (2003). Bridge topology optimisation with stress, displacement and frequency constraints. *Computers & Structures*, vol. 81, no. 3, p. 131-145, **DOI:10.1016/S0045-7949(02)00440-6**.

[24] Kim, J., Kim, J.J., Jang, I.G. (2022). Integrated topology and shape optimization of the five-spoke steel wheel to improve the natural frequency. *Structural and Multidisciplinary Optimization*, vol. 65, no. 3, p. 78, **DOI:10.1007/s00158-022-03183-3**.

[25] Duan, Z., Yan, J., Lee, I., Lund, E., Wang, G. (2019), Discrete material selection and structural topology optimization of composite frames for maximum fundamental frequency with manufacturing constraints. *Structural and Multidisciplinary*

Optimization, no. 60, p. 1741-1758, **DOI:10.1007/s00158-019-02397-2**.

[26] Oh, J.H., Ahn, Y.K., Kim, Y.Y. (2015). Maximization of operating frequency ranges of hyperbolic elastic metamaterials by topology optimization. *Structural and Multidisciplinary Optimization*, no. 52, p. 1023-1040, **DOI:10.1007/s00158-015-1288-y**.

[27] Vicente, W.M., Zuo, Z.H., Pavanello. R., Calixto, T.K.L., Picelli., R., Xie, Y.M. (2016). Concurrent topology optimization for minimizing frequency responses of two-level hierarchical structures. *Computer Methods in Applied Mechanics and Engineering*, no. 301, p. 116-136, **DOI:10.1016/j.cma.2015.12.012**.

[28] Zheng, W., Wang, Y., Zheng, Y., Da, D. (2020). Efficient topology optimization based on DOF reduction and convergence acceleration methods. *Advances in Engineering Software*, no. 149, p. 102890, **DOI:10.1016/j.advengsoft.2020.102890**.

[29] Jia, H., Beom, H.G., Wang, Y., Lin, S., Liu, B. (2011). Evolutionary level set method for structural topology optimization. *Computers & Structures*, vol. 89, no. 5-6, p. 445-454, **DOI:10.1016/j.compstruc.2010.11.003**.

[30] Lian, R., Jing, S., He, Z., Shi, Z., Song, G. (2020). An accelerating convergence rate method for moving morphable components. *Mathematical Problems in Engineering*, vol. 2020, p. 1-15, **DOI:10.1155/2020/2478292**.

[31] Joo, Y., Yu, Y., Jang, I.G. (2021). Unit module-based convergence acceleration for topology optimization using the spatiotemporal deep neural network. *IEEE Access*, no. 9, p. 149766-149779, **DOI:10.1109/ACCESS.2021.3125014**.

[32] Li, W., Zhang, X.S. (2021). Momentum-based accelerated mirror descent stochastic approximation for robust topology optimization under stochastic loads. *International Journal for Numerical Methods in Engineering*, vol. 122, no. 17, p. 4431-4457, **DOI:10.1002/nme.6672**.

[33] Du, Z., Cui, T., Liu, C., Zhang, W., Guo, Y., Guo X. (2022). An efficient and easy-to-extend Matlab code of the Moving Morphable Component (MMC) method for three-dimensional topology optimization. *Structural and Multidisciplinary Optimization*, vol. 65, no. 5, p. 158, **DOI:10.1007/s00158-022-03239-4**.

[34] Yang, C.D., Feng, J.H., Shen, Y.D. (2022). Step-size adaptive parametric level set method for structural topology optimization, Journal of Mechanical Science and Technology, no. 36, p. 5153-5164, **DOI:10.1007/s12206-022-0928-6**.

[35] Lin, H., Xu, A., Misra, A., Zhao, R. (2020). An ANSYS APDL code for topology optimization of structures with multi-constraints using the BESO method with dynamic evolution rate (DER-BESO). Structural and Multidisciplinary Optimization, no. 62, p. 2229-2254, **DOI:10.1007/s00158-020-02588-2**.

[36] Ren, C., Min, H., Ma, T., Wang F. (2020). Efficient structure crash topology optimization strategy using a model order reduction method combined with equivalent static loads, *Proceedings of the Institution of Mechanical Engineers, Part D: Journal of Automobile Engineering*, vol. 234, no. 7, p. 1897-1911, **DOI:10.1177/0954407019893841**.

[37] Huang, X., Xie, Y.M. (2010). Evolutionary topology optimization of continuum structures with an additional displacement constraint. *Structural and Multidisciplinary Optimization*, vol. 40, no. 1-6, p. 409-416, **DOI:10.1007/s00158-009-0382-4**.

[38] Fan, Z., Xia, L., Lai, W., Xia, Q., Shi, T. (2019). Evolutionary topology optimization of continuum structures with stress constraints. *Structural and Multidisciplinary Optimization*, no. 59, p. 647-658, **DOI:10.1007/s00158-018-2090-4**.